JOURNAL OF GEOPHYSICAL RESEARCH, VOL. 112, B07201, doi:10.1029/2006JB004260, 2007

Depth dependence of constitutive law parameters for shear failure of rock at local strong areas on faults in the seismogenic crust

Mitiyasu Ohnaka[1,2,3] and Aitato Kato[3]

Received 4 January 2006; revised 17 August 2006; accepted 14 December 2006; published 6 July 2007.

[1] In the framework of slip-dependent constitutive formulation, which leads to a unifying law that governs not only frictional slip failure at precut interface areas on faults but also shear fracture of intact rock at local strong areas on the faults, a thorough investigation has been made about how the constitutive law (of dimensionless form) for rock failure at local strong areas on faults is affected by seismogenic crustal conditions of effective normal stress, pore pressure, and temperature, on the basis of laboratory data on the shear fracture of granite rock obtained by Kato et al. (2003a) under crustal conditions simulated in the laboratory. It has been revealed how dimensionless constitutive law parameters distinctively vary with depth, depending on the crustal conditions simulated; consequently, the constitutive behavior including the slip-weakening phase also distinctively varies with depth. This behavior in the regime of suprahydrostatic pore pressure clearly differs from that in the regime of hydrostatic pore pressure. The results of this study are suited for implementation in a numerical code, and the constitutive properties of rock failure at local strong areas (called "asperites") on faults will be easily assimilated into numerical models of earthquake ruptures for realistic computer simulation.

Citation: Ohnaka, M., and A. Kato (2007), Depth dependence of constitutive law parameters for shear failure of rock at local strong areas on faults in the seismogenic crust, *J. Geophys. Res.*, *112*, B07201, doi:10.1029/2006JB004260.

1. Introduction

[2] It has been established to date that an earthquake source at shallow crustal depths is shear rupture instability that takes place along an inhomogeneous fault embedded in the seismogenic crust composed of rocks. At the same time, laboratory experiments have demonstrated that shear rupture of rock is governed by constitutive law. These facts enable computer simulation of earthquake generation processes in a virtual world, and a great number of such simulations have been carried out. For realistic computer simulation of earthquake ruptures, however, it is critically important to formulate the constitutive law for earthquake ruptures rationally based on solid facts, and to unravel how the constitutive law is affected by seismogenic conditions at crustal depths.

[3] The brittle, seismogenic crust and individual faults embedded therein are inherently inhomogeneous, and fault inhomogeneity has profound implications for rational constitutive formulation for earthquake ruptures [see *Ohnaka*, 2003, 2004]. There is compelling evidence that not only stress but also strength and resistance to rupture growth are inhomogeneously distributed on faults. Seismological observations and analyses [e.g., *Kanamori and Stewart*, 1978; *Aki*, 1979, 1984; *Beroza and Mikumo*, 1996; *Bouchon*, 1997; *Zhang et al.*, 2003; *Yamanaka and Kikuchi*, 2004] have commonly revealed that individual faults are heterogeneous and contain what are called "asperities" [*Lay et al.*, 1982] or "barriers" [*Aki*, 1979]. The presence of "asperities" or "barriers" on a fault physically means that a real fault comprises local strong areas of high resistance to rupture growth, with the rest of the fault having low (or little) resistance to rupture growth [see *Ohnaka*, 2004]. These seismological observations are consistent with geological observations of structural inhomogeneity and geometric irregularity for real faults described below.

[4] In general, real faults embedded in the seismogenic crust are nonplanar, being segmented and bifurcated [e.g., *Sibson*, 1986; *Wesnousky*, 1988]. In addition, individual surfaces of fault segments exhibit geometric irregularity with band-limited self-similarity [e.g., *Aviles et al.*, 1987; *Okubo and Aki*, 1987], and there are gouge layers in between fault surfaces for mature faults [*Sibson*, 1977]. These geometric irregularities and structural inhomogeneities for real faults (or fault zones) play a prominent role in causing inhomogeneous distributions of not only stresses acting on individual faults but also the fault strength and resistance to rupture growth, because these physical quantities are structure-sensitive. Consider for instance the case where a fault consists of a number of discrete segments which form an echelon array with individual segments nearly parallel to the general trend of the fault [*Segall and*

[1]Kavli Institute for Theoretical Physics, University of California, Santa Barbara, California, USA.
[2]Department of Earth Sciences, University College London, London, UK.
[3]Earthquake Research Institute, University of Tokyo, Tokyo, Japan.

0148-0227/07/2006JB004260$09.00

Pollard, 1980]. The stepover zones in such an array possibly have the highest strength, equal to fracture strength of intact rock, and the resistance to rupture growth may be high enough to impede or arrest the propagation of ruptures at these sites. In addition, nonplanar fault segment surfaces that exhibit geometric irregularity with band-limited self-similarity contain various wavelength components. When such geometrically irregular fault segment surfaces, pressed under a compressive normal stress, are sheared in the brittle regime, the prime cause of frictional resistance is the shearing strength of interlocking asperities [*Byerlee*, 1967]. In this case, the local strength at the sites of interlocking asperities is strong enough to equal the shear fracture strength of initially intact rock in the brittle regime.

[5] Thus the sites of the zones of segment stepover and/or interlocking asperities stated above are potential candidates for strong areas of high resistance to rupture growth. These sites may act as "barriers" or "asperities". When such strong areas act as "barriers", stress will build up and elastic strain energy will be accumulated at and around these sites until they break. When a large rupture breaks through these sites and links them together, they will be regarded as "asperities". Local stress drops at "asperities" on real seismic faults obtain values as high as 50 to 100 MPa [*Bouchon*, 1997; *Papageorgiou and Aki*, 1983; *Ellsworth and Beroza*, 1995], which is high enough to equal the breakdown stress drop of intact rock tested under seismogenic crustal conditions simulated in the laboratory [*Ohnaka*, 2003; *Kato et al.*, 2003a, 2004]. Strong areas such as these on a fault are required for an adequate amount of elastic strain energy to accumulate in the elastic medium surrounding the fault owing to tectonic loading. The elastic strain energy accumulated provides the driving force to bring about a large earthquake or to radiate strong motion seismic waves. The size (or magnitude) of an earthquake is prescribed by the driving force, which is in turn determined by the presence of local strong areas on the fault.

[6] Thus it is obvious that the earthquake rupture process at shallow crustal depths is not a simple one of frictional slip failure on a precut weak fault, but a more complex process including the fracture of initially intact rock on an inhomogeneous fault. Moreover, local strong areas (called "asperities") of high resistance to rupture growth on a fault play a more important role in determining the size of an earthquake than the rest of the fault with low (or little) resistance to rupture growth. The constitutive law for earthquake ruptures must therefore be formulated as a unifying law that governs not only frictional slip failure at precut interface (or frictional contact) areas on a fault but also shear fracture of intact rock at local strong areas on the fault. This very important requirement must be met when we rationally formulate the constitutive law for real earthquake ruptures.

[7] The constitutive formulations so far attempted can be categorized into two different approaches: the rate- and state-dependent formulation [e.g., *Dieterich*, 1978, 1979, 1981, 1986; *Ruina*, 1983] and the slip-dependent formulation [e.g., *Ida*, 1972; *Ohnaka et al.*, 1987; *Ohnaka and Yamashita*, 1989; *Matsu'ura et al.*, 1992]. However, the rate- and state-dependent formulation does not lead to such unifying laws as stated above, because the rate- and state-dependent law is not applicable to the instability or stability of the shear fracture process of intact rock. By contrast, the slip-dependent formulation leads to the aforementioned unifying law [see *Ohnaka*, 2003, 2004]. It is therefore very rational to assume a slip-dependent constitutive law as the governing law for earthquake ruptures.

[8] As discussed above, it is crucial to know constitutive properties for the shear fracture of intact rock at local strong areas on faults under seismogenic conditions at crustal depths. However, little attempt has been made to estimate depth profiles of the constitutive properties at such local strong areas on faults in the framework of slip-dependent constitutive formulation, though much effort has been devoted to estimating depth profiles of constitutive properties of rock friction on precut weak faults in the framework of rate- and state-dependent constitutive formulations [e.g., *Tse and Rice*, 1986; *Blanpied et al.*, 1991, 1995]. *Kato et al.* [2003a, 2004] were the first to study constitutive properties for shear fracture of intact rock under seismogenic conditions at crustal depths, and thereby estimate depth profiles of constitutive law parameters in the framework of slip-dependent constitutive formulation. However, the results are rather simplified because of a simplified analytical approach.

[9] In this paper, we will investigate in more detail, by rationally formulating the constitutive law in a dimensionless form, and by taking a numerical approach, how the slip-dependent constitutive law for shear fracture of intact rock is affected by effective normal stress, pore pressure and temperature at seismogenic, crustal depths ranging from the surface to 16 km deep in a simulated crust, and thereby specifically reestimate depth dependence of constitutive properties for rock failure at local strong areas on faults. The results are suited for implementation in a numerical code, and constitutive properties for the rupture of local strong areas on faults will be easily assimilated into numerical models for computer simulation of the earthquake generation process in realistic seismogenic environments.

2. Laboratory Data Used for Analysis

[10] To establish the constitutive law for shear fracture (or failure) of intact rock in the brittle to brittle-plastic transition regimes under seismogenic crustal conditions, it is necessary to observe carefully the entire shear failure process, during which the postfailure (or slip weakening) behavior is stabilized. The postfailure behavior can be stabilized even in the brittle regime by enhancing the stiffness of the loading system and properly choosing servocontrol variables. We constructed a sophisticated high-pressure testing apparatus having a stiff loading frame and electronic servocontrols with a 16-bit resolution digital system [*Ohnaka et al.*, 1997]. The entire system includes the load frame assembly with which servohydraulic actuators are integrated, a triaxial pressure cell, servohydraulic intensifiers (for confining pressure and pore pressure), a hydraulic power supply system, a heater and cascade temperature controller, a cooling water supply system, and a computer-automated system controller with software designed for use with multiple channel servohydraulic valves and a heater (for further details, see *Ohnaka et al.* [1997]). Using this apparatus, a great number of experiments have been conducted to observe constitutive relations for the shear failure of intact Tsukuba granite at seismogenic crustal conditions

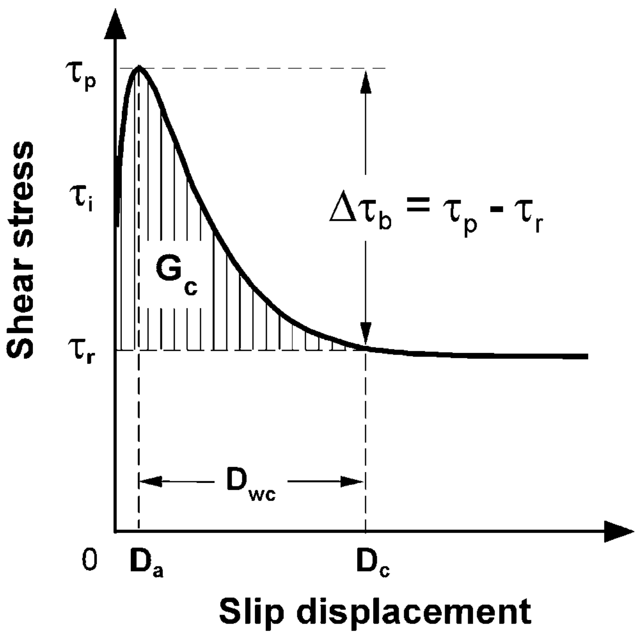

Figure 2. Schematic diagram of the laboratory-derived constitutive relation between the shear stress τ and slip displacement D. Here τ_i represents the initial strength at the onset of slip, τ_p represents the peak shear strength, $\Delta\tau_b$ represents the breakdown stress drop defined by $\Delta\tau_b = \tau_p - \tau_r$ (τ_r, residual frictional stress), D_a represents the critical displacement at which the peak shear strength is attained, and D_c represents the breakdown displacement, which is defined as the critical amount of slip required for the shear traction to degrade to the residual frictional stress. The slip-weakening displacement D_{wc} is defined by $D_{wc} = D_c - D_a$. The vertical-lined area is equal to the shear fracture energy G_c.

makes it possible to govern the stability or instability of shear fracture of intact rock [see *Ohnaka*, 2003, 2004]. The formulation presumes that the shear traction τ along the macroscopic rupturing surfaces degrades with ongoing slip D (see Figure 2), with its functional form being affected by other parameters such as slip rate $\dot{D}$. The law is in general expressed as [*Ohnaka*, 1996, 2004; *Ohnaka et al.*, 1997]

$$\tau = f\left(D; \dot{D}, \lambda_c, \sigma_n^{eff}, T, \mathrm{CE}\right) \tag{1}$$

where f represents the constitutive relation between τ and D, and the constitutive relation may be affected by not only $\dot{D}$ but also such parameters as the scaling parameter λ_c, effective normal stress σ_n^{eff}, temperature T, and the chemical effect of interstitial pore water CE. The effective normal stress is defined by $\sigma_n^{eff} = \sigma_n - P$, where σ_n is normal stress, and P is pore pressure. An essential feature of this formulation is that slip displacement is an independent variable and that the transient response of the shear traction to the displacement is fundamentally important. The effect of slip rate is secondary compared with the primary effect of displacement.

[15] The slip-dependent constitutive relation derived from laboratory experiments on the shear rupture of rock is commonly represented as illustrated in Figure 2. In Figure 2, τ_i represents the initial strength at the onset of slip, τ_p is the peak shear strength, $\Delta\tau_b$ is the breakdown stress drop defined by $\Delta\tau_b = \tau_p - \tau_r$ (τ_r, residual frictional stress), D_a is the critical displacement at which the peak shear strength is attained, and D_c is the breakdown displacement, defined as the critical amount of slip required for the shear traction to degrade to the residual frictional stress. The slip-weakening displacement D_{wc} is defined by $D_{wc} = D_c - D_a$. The vertical-lined area in Figure 2 is equal to the apparent shear rupture energy G_c defined by [*Palmer and Rice*, 1973]

$$G_c = \int_0^{D_c} [\tau(D) - \tau_r] dD \tag{2}$$

from which it can intuitively be understood that the slip-dependent constitutive law automatically satisfies the Griffith energy balance fracture criterion. Since G_c represents the energy required for the rupture front to further grow, the resistance to rupture growth is defined as G_c.

[16] In this paper, focus is placed on how the slip-dependent constitutive law is affected by the effective normal stress, pore water pressure, and temperature in the seismogenic layer at crustal depths. The effects of $\dot{D}$, λ_c, σ_n^{eff}, T, and CE are implicitly exerted on the law through the constitutive law parameters τ_i, τ_p, $\Delta\tau_b$, D_a, and D_c. These constitutive law parameters are affected by the effective normal stress, pore water pressure, and temperature, which in turn are functions of position $\boldsymbol{r}$ in the crust. We thus assume that the laboratory-derived constitutive relation between τ and D at a position $\boldsymbol{r}$ is expressed as [*Ohnaka*, 1996]

$$\tau(D, \boldsymbol{r}) = \tau_p(\boldsymbol{r}) - \Delta\tau_{b\infty}(\boldsymbol{r}) \cdot \left\{1 - h(D, \boldsymbol{r}) \exp\left[-A(\boldsymbol{r})B(\boldsymbol{r})\left(\frac{D}{D_a(\boldsymbol{r})} - 1\right)\right]\right\} \tag{3}$$

where

$$h(D, \boldsymbol{r}) = 1 + A(\boldsymbol{r}) \log\left(1 + B(\boldsymbol{r})\left(\frac{D}{D_a(\boldsymbol{r})} - 1\right)\right) \tag{4}$$

In equations (3) and (4), $\Delta\tau_{b\infty}$ is the breakdown stress drop defined by $\Delta\tau_{b\infty} = \tau_p - \tau_{r\infty}$ ($\tau_{r\infty}$ is the residual friction stress as $D \to \infty$), and $A(\boldsymbol{r})$ and $B(\boldsymbol{r})$ are dimensionless parameters which are functions of position $\boldsymbol{r}$ on the fault.

[17] Here we define an effective breakdown displacement D_c^{eff} as the slip displacement at which the relation $\tau = \tau_{r\infty} + \chi\Delta\tau_{b\infty}$ holds, where χ is a fixed numerical parameter (for instance, 0.1) that has been introduced to define D_c^{eff}. The corresponding effective breakdown stress drop $\Delta\tau_b^{eff}$ is given by $\Delta\tau_b^{eff} = (1 - \chi)\Delta\tau_{b\infty}$. We will hereafter use the symbols D_c^{eff} and $\Delta\tau_b^{eff}$ in place of D_c and $\Delta\tau_b$, respectively.

[18] If the constitutive law parameters τ_p, τ_i, $\Delta\tau_b^{eff}$, D_a, and D_c^{eff} are known as functions of position $\boldsymbol{r}$, the parameters

$A(\boldsymbol{r})$ and $B(\boldsymbol{r})$ can be determined by solving the following simultaneous equations [*Ohnaka*, 1996]:

$$\left\{1 + A(\boldsymbol{r})\log\left[1 + B(\boldsymbol{r})\left(\frac{D_c^{\text{eff}}(\boldsymbol{r})}{D_a(\boldsymbol{r})} - 1\right)\right]\right\} \cdot \exp\left[-A(\boldsymbol{r})B(\boldsymbol{r})\left(\frac{D_c^{\text{eff}}(\boldsymbol{r})}{D_a(\boldsymbol{r})} - 1\right)\right] = \chi \quad (5)$$

and

$$1 - [1 + A(\boldsymbol{r})\log(1 - B(\boldsymbol{r}))]\exp[A(\boldsymbol{r})B(\boldsymbol{r})] = R(\boldsymbol{r}) \quad (6)$$

where

$$R(\boldsymbol{r}) = \frac{\tau_p(\boldsymbol{r}) - \tau_i(\boldsymbol{r})}{\Delta\tau_b^{\text{eff}}(\boldsymbol{r})/(1-\chi)} \quad (7)$$

[19] If we further define the dimensionless shear stress σ by $\sigma = \tau/\tau_p(\boldsymbol{r})$, and the dimensionless slip displacement d by $d = D/D_a(\boldsymbol{r})$, equation (3) is rewritten as

$$\sigma(d, \boldsymbol{r}) = 1 - S(\boldsymbol{r})\{1 - [1 + A(\boldsymbol{r})\log(1 + B(\boldsymbol{r})(d-1))] \cdot \exp[-A(\boldsymbol{r})B(\boldsymbol{r})(d-1)]\} \quad (8)$$

where

$$S(\boldsymbol{r}) = \frac{\Delta\tau_b^{\text{eff}}(\boldsymbol{r})/(1-\chi)}{\tau_p(\boldsymbol{r})}. \quad (9)$$

If $A(\boldsymbol{r})$, $B(\boldsymbol{r})$, and $S(\boldsymbol{r})$ are evaluated at any position $\boldsymbol{r}$ on a fault embedded in the seismogenic crust, equation (8) completely specifies the relation between σ and d on the fault, and hence the constitutive relation between τ and D on the same fault can be uniquely determined.

[20] Laboratory experiments [*Ohnaka*, 2003] on rock fracture and frictional slip failure clearly show that the displacement parameters D_a, D_c^{eff} and D_{wc} (= $D_c^{\text{eff}} - D_a$) are not independent but dependent on one another. In other words, there are direct proportional relationships between D_a, D_{wc} and D_c^{eff}; that is [*Ohnaka*, 2003],

$$D_{wc} = c_1 D_c^{\text{eff}} \quad (10)$$

and

$$D_a = c_2 D_c^{\text{eff}} \quad (11)$$

where $c_1 + c_2 = 1$ and c_1 and c_2 are numerical constants. The laboratory experiments [*Ohnaka*, 2003] also demonstrate that the fundamental cause of the scaling property of the displacement parameters D_a, D_{wc}, and D_c^{eff} lies in the characteristic length λ_c, defined as the predominant wavelength that represents geometric irregularity of the shear-rupturing surfaces in the slip direction. Specifically, D_c^{eff} scales with λ_c in accordance with the following relation [*Ohnaka*, 2003]:

$$D_c^{\text{eff}} = \mathrm{K}\left(\frac{\Delta\tau_b^{\text{eff}}}{\tau_p}\right)^m \lambda_c \quad (12)$$

where K and m are constants in the brittle regime. As is obvious from equations (10), (11) and (12), D_a and D_{wc} also scale with λ_c (for details, see *Ohnaka* [2003]).

4. Depth Dependence of Constitutive Law Parameters

[21] In the previous analysis, *Kato et al.* [2004] implicitly assumed a simplified slip-weakening model, in which the slip-strengthening phase before the peak strength is attained at $D = D_a$ is completely disregarded, and the roles of the parameters τ_i and D_a are not considered in the model. Though such a simplified slip-weakening model is useful, note that the model necessarily leads to a singularity of slip acceleration near the front of a dynamically propagating rupture [*Ida*, 1973], which is physically unrealistic. To avoid such an unrealistic singularity of slip acceleration, the constitutive law must be formulated so as to incorporate the slip-strengthening phase [*Ida*, 1973; *Ohnaka and Yamashita*, 1989]. Hence the parameters τ_i and D_a cannot be ignored in the constitutive formulation when we discuss strong motion source parameters such as the peak slip velocity and acceleration in dynamic rupture regime in quantitative terms [*Ohnaka and Yamashita*, 1989]. In this section, we evaluate depth dependence of constitutive law parameters, assuming a more complete formulation of the constitutive law expressed by equation (3) or (8).

[22] The dimensionless form (8) of the constitutive law is uniquely determined as a function of depth $\boldsymbol{r}$ if the parameters $S(\boldsymbol{r})$, $A(\boldsymbol{r})$ and $B(\boldsymbol{r})$ are known. It is therefore critical to identify depth profiles of these parameters in the seismogenic zone. We investigate specifically how the constitutive law parameters S, A, and B vary with depth, depending on the seismogenic, crustal conditions of σ_n^{eff}, P, and T, using laboratory data published by *Kato et al.* [2003a].

[23] To observe how the dimensionless quantity S defined by equation (9) is affected by σ_n^{eff}, P, and T at crustal depths, $\Delta\tau_b^{\text{eff}}/\tau_p$ is plotted as a function of depth in Figure 3. The broken lines in Figure 3 indicate five-point moving averages for each pore pressure regime. One can see from Figure 3 that $\Delta\tau_b^{\text{eff}}/\tau_p$ decreases with depth, and is greater in the suprahydrostatic pore pressure regime than in the hydrostatic pore pressure regime. This difference is ascribed to the difference in the effective normal stress σ_n^{eff} due to different pore pressures. This is confirmed in Figure 4, which shows a plot of $\Delta\tau_b^{\text{eff}}/\tau_p$ against σ_n^{eff} for two different sets of data obtained under the two different pore pressure regimes. One can clearly see that when $\Delta\tau_b^{\text{eff}}/\tau_p$ is plotted against σ_n^{eff}, the two different sets of data are aligned with each other in spite of the differences in pore pressure and temperature between the two.

[24] To solve simultaneous equations (5) and (6) in order to find a set of numerical solutions for $A(\boldsymbol{r})$ and $B(\boldsymbol{r})$ at a depth $\boldsymbol{r}$, we have to know depth distributions of the parameters $R = (\tau_p - \tau_i)/[\Delta\tau_b^{\text{eff}}/(1 - \chi)]$ and D_c^{eff}/D_a. To observe how the dimensionless quantity R varies with depth, depending on the crustal conditions of σ_n^{eff}, P, and T, $(\tau_p - \tau_i)/\Delta\tau_b^{\text{eff}}$ is plotted against depth in Figure 5. The broken lines in Figure 5 indicate five-point moving averages for each pore pressure regime. It is found from Figure 5 that $(\tau_p - \tau_i)/\Delta\tau_b^{\text{eff}}$ increases with depth in the hydrostatic pore pressure regime, while it is insensitive to depth in the

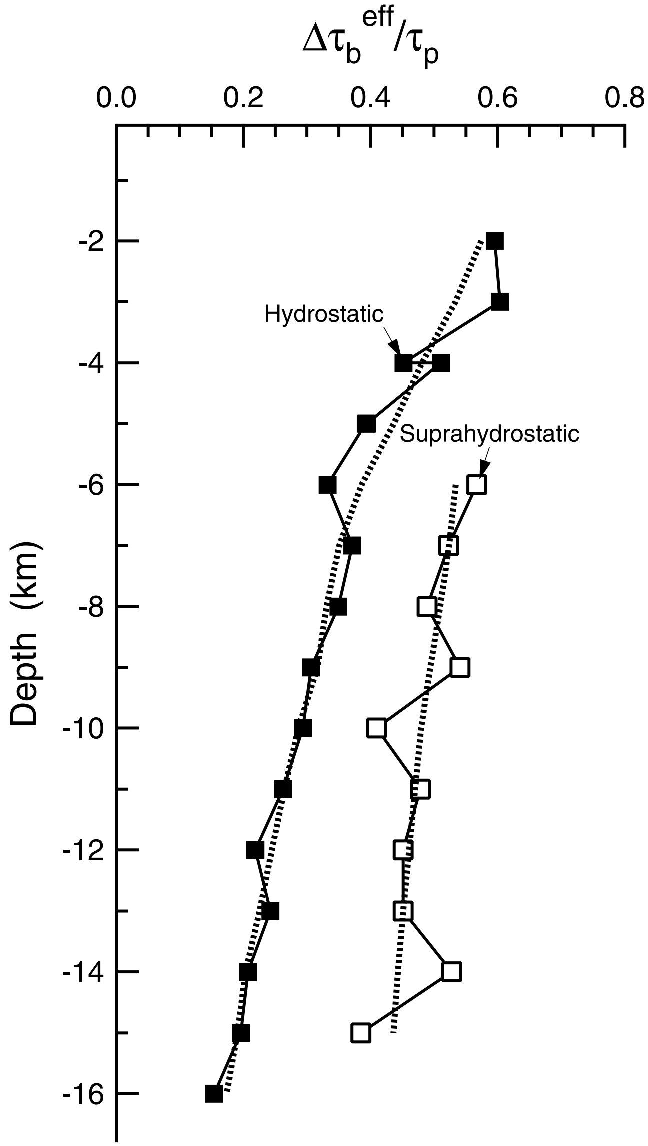

Figure 3. Plot of $\Delta\tau_b^{eff}/\tau_p$ against crustal depth for data obtained under hydrostatic and suprahydrostatic pore pressures.

suprahydrostatic pore pressure regime. It is also found that $(\tau_p - \tau_i)/\Delta\tau_b^{eff}$ is greater in the hydrostatic pore pressure regime than in the suprahydrostatic pore pressure regime, which is ascribed to the difference in σ_n^{eff} between the two regimes due to different pore pressures. This is confirmed in Figure 6, which shows a plot of $(\tau_p - \tau_i)/\Delta\tau_b^{eff}$ against σ_n^{eff} for two different sets of data obtained in the two different pore pressure regimes. One can see from Figure 6 that these different sets of data are aligned with each other in spite of the differences in pore pressure and temperature.

[25] To evaluate how D_c^{eff}/D_a varies with depth, we first determine to what extent the ratio D_c^{eff}/D_a is affected by σ_n^{eff}, P, and T. Since D_{wc} is defined as $D_{wc} = D_c^{eff} - D_a$, the ratio D_c^{eff}/D_a is uniquely related to the ratio D_{wc}/D_c^{eff} $(= 1 - D_a/D_c^{eff})$, and hence it suffices to investigate how the ratio D_{wc}/D_c^{eff} is affected by σ_n^{eff}, P, and T. Figure 7 shows a plot of $c_1 = D_{wc}/D_c^{eff}$ against the peak shear strength τ_p for data on frictional slip failure and the shear fracture of intact Tsukuba granite tested in the brittle regime (where temperature ranges from room temperature to roughly 300°C). These data were taken from earlier papers [*Ohnaka and Shen*, 1999; *Ohnaka*, 2003], with some unpublished data (2003). Figure 7 shows that D_{wc}/D_c^{eff} does not depend on τ_p. Since τ_p is an increasing function of σ_n^{eff} in the brittle regime, one can see from Figure 7 that the ratio D_c^{eff}/D_a is not only unaffected by the peak shear strength but also unaffected by the effective normal stress in the brittle regime. Figure 7 also shows that the ratio D_{wc}/D_c^{eff} has a constant value of 0.8 (which corresponds to $D_c^{eff}/D_a = 5$) for both the shear fracture of intact rock and frictional slip failure on a precut fault. This suggests that the shear fracture of intact rock and frictional slip failure can both be unified in a consistent manner in the framework of slip-dependent constitutive formulation [*Ohnaka*, 2003].

[26] Figure 8 shows how D_c^{eff}/D_a $(= 1/c_2)$ varies with depth. Figure 8 indicates that D_c^{eff}/D_a does not significantly vary with depth at depths shallower than roughly 10 km, whereas it increases at greater depths. One can see from Figure 8 that D_c^{eff}/D_a at depths shallower than 10 km is significantly unaffected by pore pressure within the experimental errors. At greater depths, however, it is affected by pore pressure; in other words, D_c^{eff}/D_a at depths greater than 10 km is affected more sensitively in the suprahydrostatic pore pressure regime than in the hydrostatic pore pressure regime. Note that the ratios of one displacement parameter D_a, D_{wc}, or D_c^{eff} to another are scale-independent [*Ohnaka*, 2003]. This can easily be confirmed from Figure 9, which shows a plot of $c_1 = D_{wc}/D_c^{eff}$ against the effective breakdown displacement D_c^{eff} for data on frictional slip failure and shear fracture of intact Tsukuba granite tested in the brittle regime [*Ohnaka*, 2003]. From Figure 9, one can see that $c_1 = D_{wc}/D_c^{eff}$ does not depend on D_c^{eff}. This means that the ratio D_{wc}/D_c^{eff} is scale-independent, despite the fact that each displacement parameter D_c^{eff} or D_{wc} is scale-dependent as mentioned in section 3. Likewise, the ratio D_c^{eff}/D_a $(= D_c^{eff}/(D_c^{eff} - D_{wc}))$ is also scale-independent.

[27] We can thus summarize two important facts about the displacement parameters D_a, D_{wc}, and D_c^{eff} as follows: (1) the ratios of one displacement parameter D_a, D_{wc}, or D_c^{eff} to another are constant, and neither scale-dependent nor dependent on ambient conditions such as the effective normal stress and temperature in the brittle regime, and (2) D_c^{eff}/D_a has a universal, constant value of roughly 5 within experimental error in the brittle regime (corresponding to a depth range down to roughly 10 km). The value of 5 for D_c^{eff}/D_a in the brittle regime agrees with that obtained in previous experiments [see *Ohnaka*, 2003]. For the hydrostatic pore pressure regime, we thus assume that D_c^{eff}/D_a has a constant value of 5 within a depth range down to 11 km, and at greater depths increases as listed in Table 1 (see also Figure 8). For the suprahydrostatic pore pressure regime, we consider the fact that D_c^{eff}/D_a is more sensitively affected by pore water pressure at greater depths, and hence we assume that D_c^{eff}/D_a has the same value of 5 within a depth range down to 9 km, and at greater depths increases as listed in Table 2 (see also Figure 8).

[28] Using values listed in Tables 1 and 2 for D_c^{eff}/D_a and R as a function of depth, we can now solve simultaneous

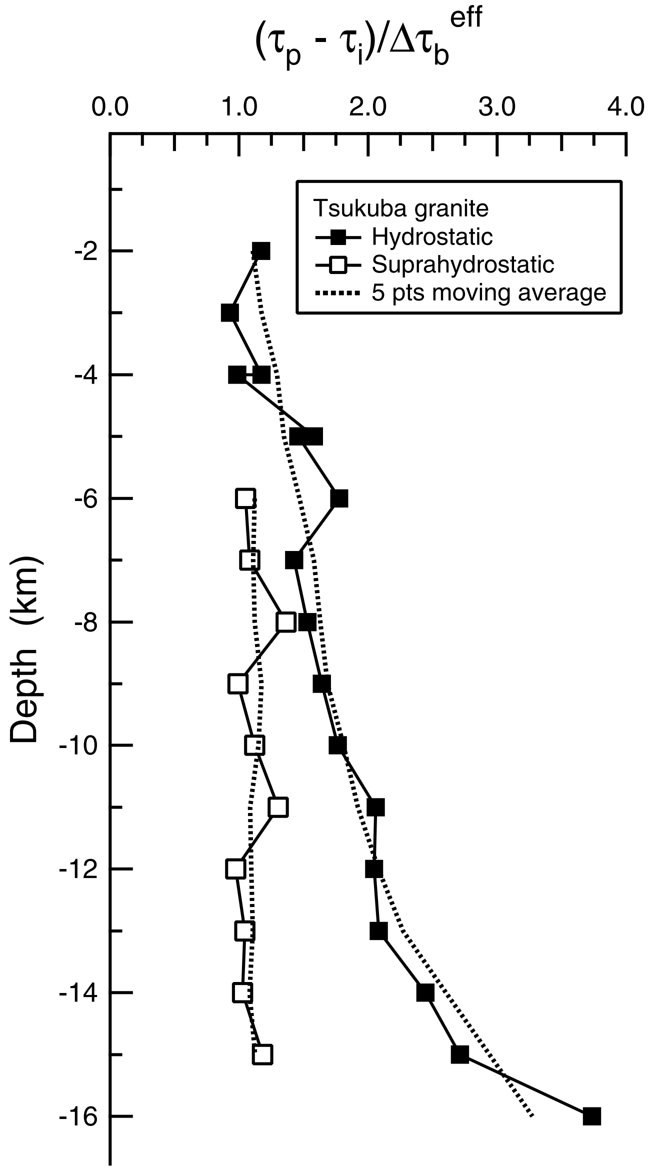

Figure 5. Plot of $(\tau_p - \tau_i)/\Delta\tau_b^{eff}$ against crustal depth for data obtained under hydrostatic and suprahydrostatic pore pressures.

5. Discussion

[31] As stated in sections 1 and 3, the slip-dependent constitutive law is the only formulation that makes it possible to govern the stability or instability of the shear fracture which possibly occurs at local strong areas called "asperities" on faults, and the law automatically satisfies the Griffith energy balance fracture criterion. In addition, formulation of the governing law as a slip-dependent constitutive law is more appropriate than any other formulation for accounting for scale-dependent physical quantities inherent in the rupture quantitatively [*Ohnaka*, 2006]. This is because the scale-dependent physical quantities scale straightforwardly with the breakdown displacement D_c^{eff}, which is directly related to the geometric length of the coherent zone of rupture breakdown [see *Ohnaka*, 2000, 2003, 2004]. Note that D_c^{eff} is by definition the slip displacement at the end of the breakdown process and that the parameter D_c^{eff} needed to account for the scale-dependent physical quantities is inherently incorporated into the slip-dependent law. Thus the slip-dependent constitutive law is a generalized, more universal law than the Griffith fracture criterion, in the sense that the physical scaling property is incorporated into the slip-dependent law.

[32] In the framework of slip-dependent constitutive formulation, we have estimated depth distributions of the dimensionless constitutive law parameters S, A, and B at strong areas called "asperities" on faults from experimental data [*Kato et al.*, 2003a]. These estimates enable one to specify depth distributions of the dimensionless constitutive relation between σ and d from equation (8). Figures 13 and 14 show how constitutive relations thus derived between σ and d change with depth, in the hydrostatic and suprahydrostatic pore pressure regimes, respectively. These relations have been calculated using the values for S, A, and B listed in Tables 1 and 2. One can see clearly from Figures 13 and 14 that slip-weakening behavior, after peak strength has been attained, is observed at all depths down to 15–16 km; however, this slip-weakening behavior (or the constitutive relation between σ and d) distinctively changes with depth, with variations of lithostatic pressure, pore pressure, and temperature. These distinctive features have to be assimilated into numerical models for computer simulation of the earthquake generation process in realistic seismogenic environments.

[33] The dimensionless shear traction σ is converted to a dimensional shear traction τ by the relation $\tau = \tau_p\sigma$, and the dimensionless slip displacement d is converted to a dimensional slip displacement D by the relation $D = D_a d$. In order to convert the dimensionless form of the constitutive relation to its dimensional form at individual depths, we need to know depth profiles of τ_p and D_a under the simulated seismogenic, crustal conditions. Figure 15 shows experimental results of *Kato et al.* [2003a], indicating how τ_p and D_c^{eff} for the shear fracture of intact Tsukuba granite vary with depth at the simulated crustal conditions of temperature, and lithostatic pressure in the hydrostatic and suprahydrostatic pore pressure regimes shown in Figure 1. *Kato et al.* [2004] empirically derived equations expressing τ_p and D_c^{eff} as functions of the effective normal stress and temperature in the hydrostatic pore pressure regime.

[34] In section 1 we argued that real earthquake faults in the crust are inherently inhomogeneous [see also *Ohnaka*, 2004] and that these inhomogeneous faults comprise local strong areas (called "asperities" or "barriers") of high resistance to rupture growth, with the rest of the faults having low (or little) resistance to rupture growth. Since τ_p shown in Figure 15 is the shear fracture strength of intact granite obtained at seismogenic crustal conditions, it represents the highest possible value for the strength of such strong areas on faults embedded in the seismogenic crust. Note that the shear fracture strength is the upper limit of frictional strength on a precut interface, which can easily be proven in terms of the microcontact physics of a sliding interface in intimate contact [*Ohnaka*, 1996]. The highest possible value for the strength at strong areas on faults is greatly affected by pore pressure. Therefore the dimensional shear traction τ, to which the dimensionless shear traction σ

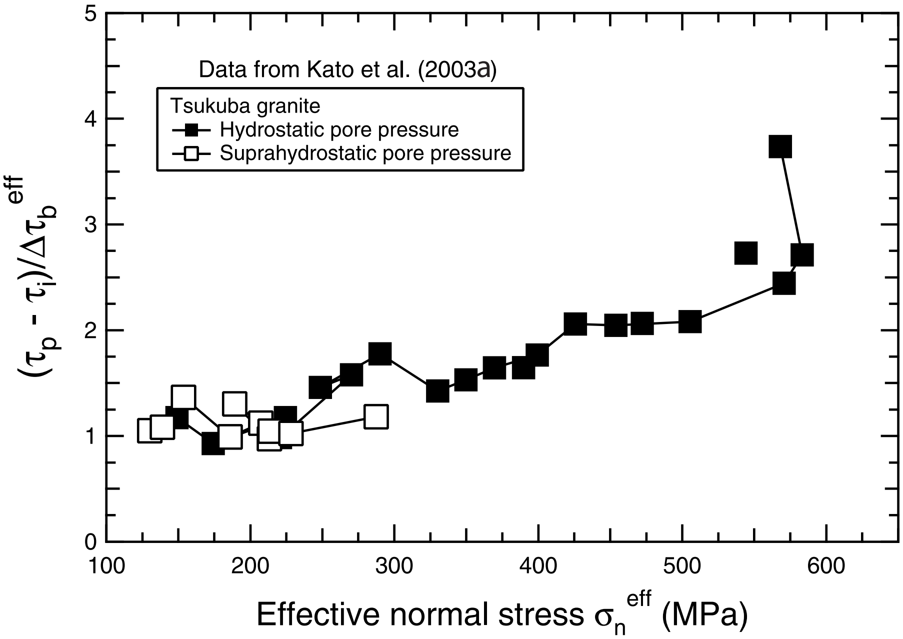

Figure 6. Plot of $(\tau_p - \tau_i)/\Delta\tau_b^{eff}$ against the effective normal stress σ_n^{eff} for data obtained in the hydrostatic and suprahydrostatic pore pressure regimes.

is converted by $\tau = \tau_p\sigma$, is also greatly affected by the mechanical effect of pore pressure. Indeed, τ_p in the hydrostatic pore pressure regime is much higher than that in the suprahydrostatic pore pressure regime (Figure 15).

[35] The constitutive law parameter D_a plays a key role in converting the dimensionless parameter d to the corresponding displacement parameter D, which is scale-dependent. Hence it is important to observe how and to what extent D_a is affected by seismogenic, crustal conditions. It has been unknown until now, however, how D_a varies with depth at seismogenic, crustal conditions, because the role of D_a has been overlooked. It is therefore worthwhile to present it. A plot of D_a against depth is shown in Figure 15 for the data set taken from *Kato et al.* [2003a]. One can see from Figure 15 that D_a can be regarded as virtually constant over a depth range down to 16 km; in other words, it is neither appreciably affected by effective normal stress or temperature, nor affected by whether failure occurs in the hydrostatic pore pressure regime or in the suprahydrostatic pore pressure regime. This finding is important and noteworthy because D_c^{eff} exhibits contrasting behavior in a depth range roughly from

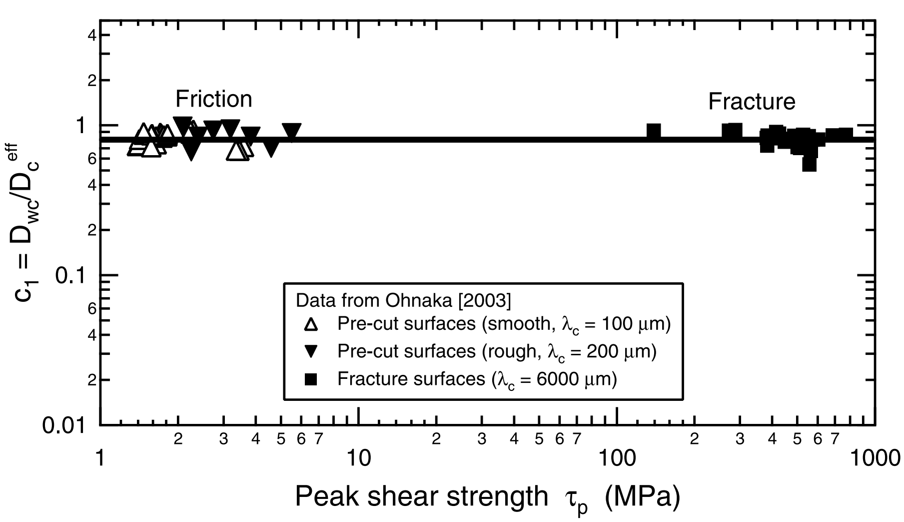

Figure 7. Plot of $c_1 = D_{wc}/D_c^{eff}$ against the peak shear strength τ_p for frictional slip failure and shear fracture of intact granite tested in the brittle regime.

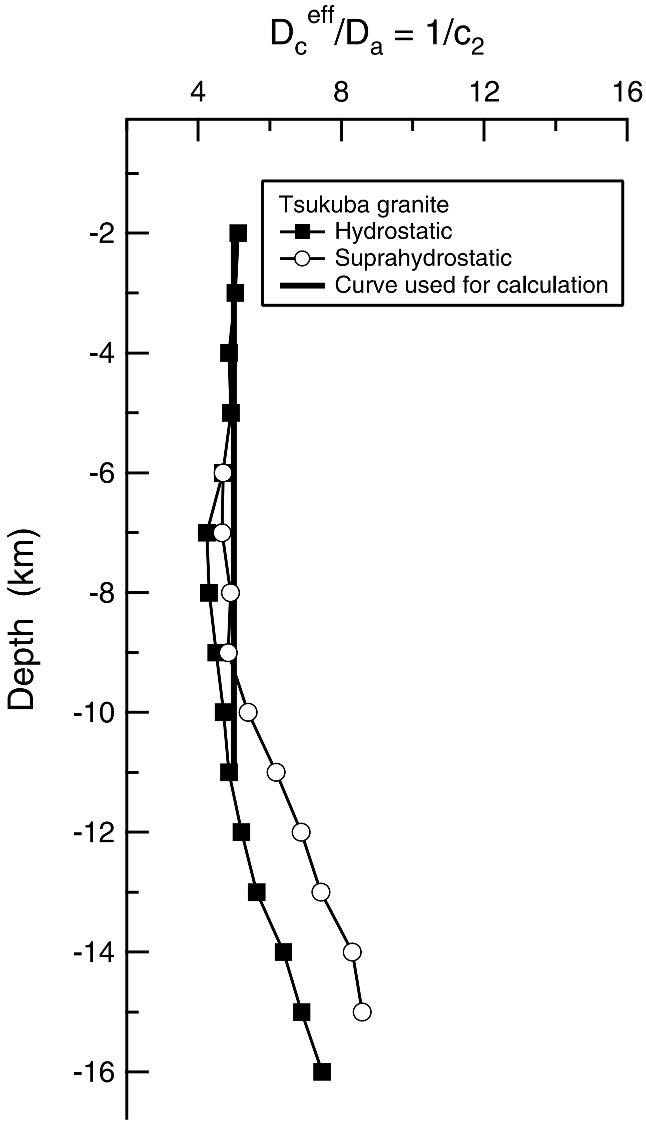

Figure 8. Plot of D_c^{eff}/D_a (= $1/c_2$) against crustal depth for data obtained in the hydrostatic and suprahydrostatic pore pressure regimes.

10 to 16 km, where it increases with depth (see Figure 15). It has been shown that the increase in D_c^{eff} with depth in the range from 10 to 16 km is ascribed to the effect of temperature above 300°C [*Kato et al.*, 2003a].

[36] D_a (and D_c^{eff}) shown in Figure 15 are the critical displacements on the shear rupture surfaces of intact Tsukuba granite samples (circular cylinders 40 mm long and 16 mm in diameter) tested in the laboratory. Since D_a and D_c^{eff} are scale-dependent, it is meaningless to compare their absolute values obtained in the laboratory straightforwardly with those of earthquake ruptures that occur on crustal faults of much larger scale. Although it has been found that D_a is neither influenced by such crustal conditions as the effective normal stress and temperature, nor influenced by whether failure occurs in the hydrostatic or suprahydrostatic pore pressure regime, D_a depends significantly on the characteristic length λ_c that represents the predominant wavelength of geometric irregularity of the shear-rupturing surfaces. As noted in section 3, D_a scales with D_c^{eff} in the brittle regime in accordance with equation (11).

[37] Since D_c^{eff} is directly related to the geometric length of the coherent zone of rupture breakdown, the critical amount of slip required for a larger asperity to break down is necessarily larger. Consider for instance a simple situation where two asperities on a fault are interlocked. In order to shear the fault in this situation, it is necessary for these interlocking asperities to fracture (when the compressive normal stress is sufficiently high), or alternatively to slide over each other (when the normal stress is sufficiently low). When a geometrically larger asperity is fractured, a longer predominant wavelength is necessarily contained in the irregular rupturing surfaces of the asperity because of fractal nature involved when the other conditions are equal, and D_c^{eff} scales with the characteristic length λ_c defined as the predominant wavelength of the geometric irregularity in the slip direction, according to equation (12) [*Ohnaka*, 2003]. On the other hand, when two interlocking asperities slide over each other to cause frictional slip failure, D_c^{eff} scales with the predominant length λ_c determined from the slip distance required for one asperity to slide over the other. In either case, a large amount of slip is necessary for a large

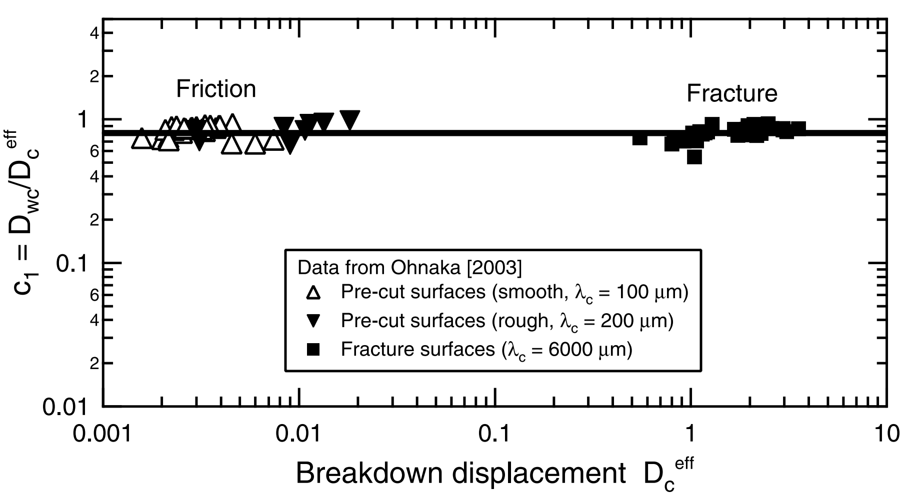

Figure 9. Plot of $c_1 = D_{wc}/D_c^{eff}$ against the effective breakdown displacement D_c^{eff} for frictional slip failure and shear fracture of intact granite tested in the brittle regime.

Table 1. Changes in Dimensionless Constitutive Law Parameters With Depth Under the Hydrostatic Pore Pressure Regime[a]

Depth, km	S	R	D_c^{eff}/D_a	A	B
2	0.6379	0.9943	5.0000	4.9634	0.1821
3	0.5931	1.0567	5.0000	3.3733	0.2617
4	0.5347	1.1655	5.0000	2.3603	0.3645
5	0.4849	1.2114	5.0000	2.1333	0.4001
6	0.4285	1.3196	5.0000	1.7816	0.4720
7	0.3896	1.4209	5.0000	1.5758	0.5280
8	0.3674	1.4652	5.0000	1.5075	0.5498
9	0.3519	1.5163	5.0000	1.4400	0.5732
10	0.3180	1.6279	5.0000	1.3238	0.6188
11	0.2942	1.7273	5.0000	1.2455	0.6541
12	0.2722	1.8718	5.2073	1.0097	0.7520
13	0.2504	2.0424	5.6314	0.7843	0.8582
14	0.2264	2.3440	6.3809	0.5940	0.9488
15	0.2120	2.6479	6.8876	0.5194	0.9784
16	0.1925	2.9456	7.4705	0.4605	0.9921

[a][illegible]r the definition of symbols S, R, D_c^{eff}/D_a, A, and B used, see text.

[illegible]ty to fracture or to slide over the other, and the critical [illegible]t of slip required for shear fracture or frictional slip [illegible] is related to λ_c. These two cases are inclusively [illegible]d to by the term "breakdown", and relation (12) has [illegible]rived empirically from laboratory data on both shear [illegible] and frictional slip failure. Note therefore that [illegible](12) is a formulation of the fact that the critical [illegible]of slip required for a larger asperity to "break [illegible]s necessarily larger (for details, see *Ohnaka* [illegible]his scaling relation makes it possible to account [illegible]dependent physical quantities inherent in the [illegible]er a broad-scale range in quantitative terms, in [illegible]d consistent manner [*Ohnaka*, 2003]. Therefore [illegible] incorporated into physical models of earth[illegible]es for realistic simulations.

[illegible]eral, a large fault tends to include geometri[illegible]al areas of high resistance to rupture growth [illegible]ense. The irregular rupture surfaces of such [illegible]ge local areas contain a long predominant [illegible]onent λ_c because such rupture surfaces [illegible]e. When a number of str[illegible]g areas (or [illegible]rent sizes having hi[illegible] resistance to r[illegible]mogeneously d[illegible]uted on a fault, the [illegible]ach asperity to be broke[illegible]ity to another, and therefo[illegible] inhomogeneously on

Table 2. Changes [illegible]nless Constitutive Law Parameters With Depth Under the [illegible]hydrostatic Pore Pressure Regime[a]

Depth, km	S	R	D_c^{eff}/D_a	A	B
6	0.5936	[illegible]	5.0000	4.4725	0.2009
7	[illegible]	[illegible]	5.0000	4.8619	0.1857
[illegible]	[illegible]561	1.0093	[illegible]0000	4.4089	0.2036
[illegible]	[illegible].5491	1.0549	5.0[illegible]	3.4015	0.2597
[illegible]	0.5327	1.0355	5.3993	[illegible]0262	0.6294
[illegible]	0.5222	0.9777	6.1837	[illegible]	0.7875
[illegible]	0.5116	0.9840	6.8782	0.645[illegible]	[illegible]7842
[illegible]	0.5011	0.9950	7.4397	0.4961	[illegible]
[illegible]	0.4922	0.9732	8.3092	0.3983	[illegible]
[illegible]15	0.4840	1.0106	8.5930	0.3996	0.919[illegible]

[a]For the definition of symbols S, R, D_c^{eff}/D_a, A, and B used, see text.

the fault. O[illegible] the largest [illegible] responsible [illegible] on the faul[illegible] from the f[illegible] capable of [illegible] energy stor[illegible] earthquake [illegible] capable of su[illegible] [see *Ohnaka*[illegible] seismologica[illegible] seismologica[illegible] *Takeo*, 1997; [illegible] *et al.*, 2003; [illegible] larger earthq[illegible] 2003], and *D*[illegible]

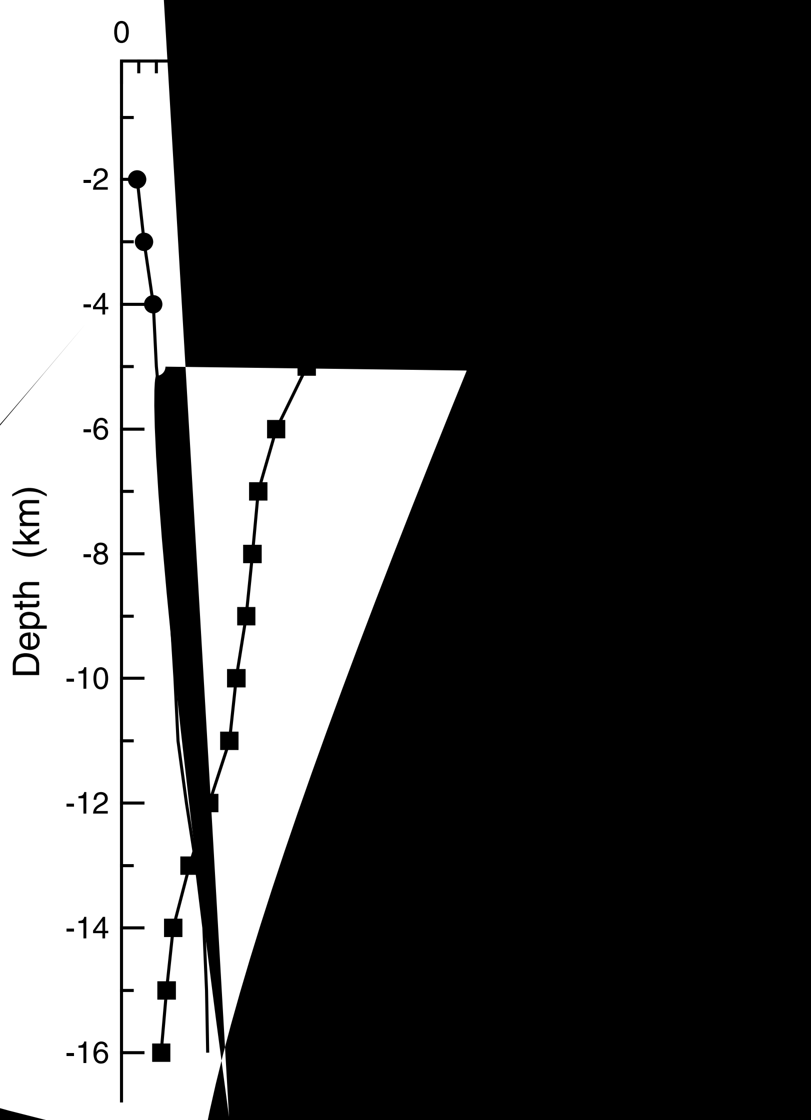

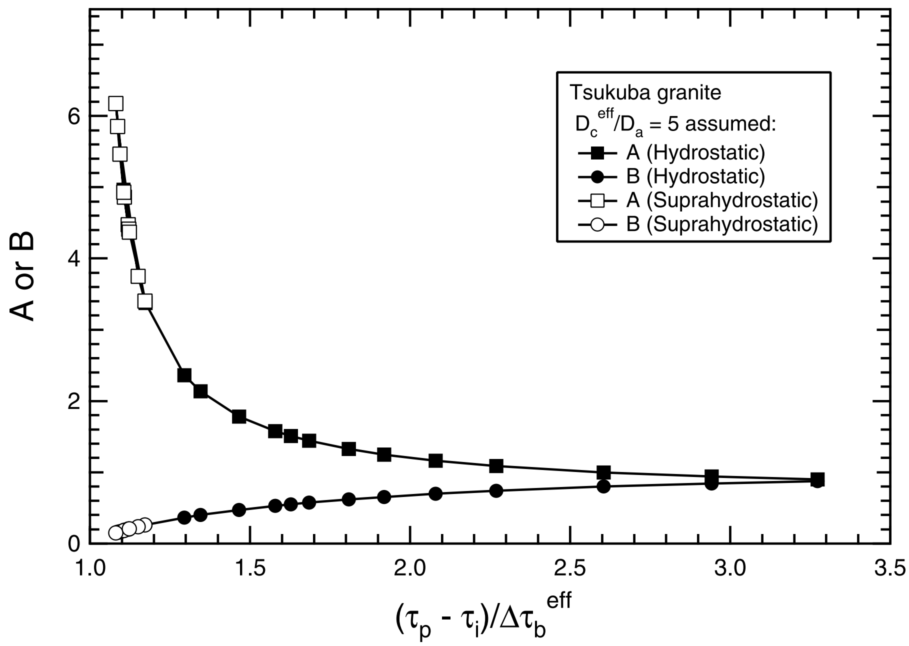

Figure 11. Relation of A or B to $(\tau_p - \tau_i)/\Delta\tau_b^{eff}$. The case for which a value of $D_c^{eff}/D_a = 5$ has been assumed is shown.

of the order of 1 m or more, which is 10^3 times larger than D_c^{eff} measured for the shear fracture of granite samples in the laboratory (for details, see *Ohnaka* [2003]). A correct estimate of the amount of D_c^{eff} is important not only in evaluating the apparent rupture energy (or the resistance to rupture growth) but also in evaluating D_a for an earthquake. D_a can be estimated from equation (11): for instance, D_a = 20 cm if D_c^{eff} is assumed to be 1 m in the brittle regime. Note therefore that the amount of D_a is not negligible.

[39] It has been found that the parameters c_1, c_2, K, and m for the shear fracture of intact rock in the brittle regime (at temperatures below 300°C) have constant values equal to those for frictional slip failure. The existing data suggest, however, that some of those parameters depend on temperature above 300°C (Figure 8; see also *Ohnaka* [2003]).

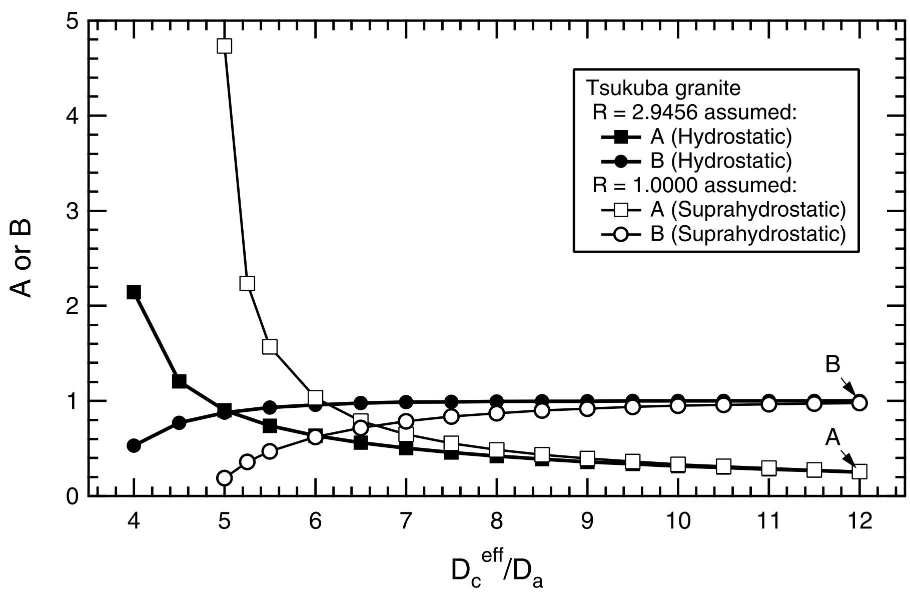

Figure 12. Relation of A or B to D_c^{eff}/D_a. The two cases where R = 1.0000 and 2.9456 have been assumed are shown for hydrostatic and suprahydrostatic pore pressures.

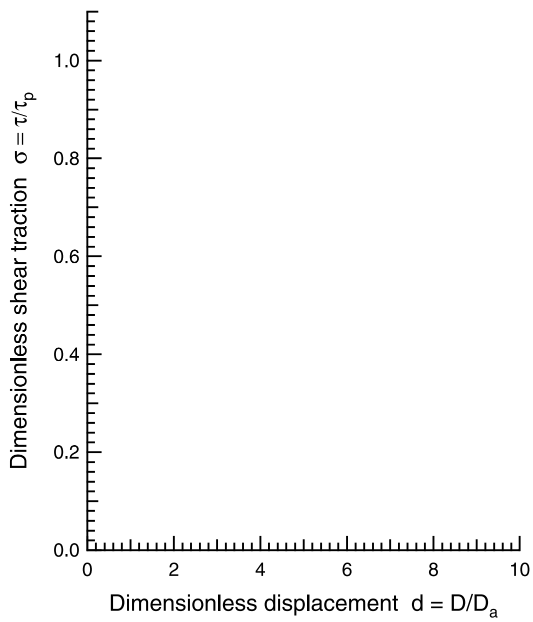

Specifically, $1/c_2$ ($= D_c^{eff}/D_a$) can be regarded as constant in a depth range to 9 km, below which it increases with depth, in the suprahydrostatic pore pressure regime, while it can be regarded as constant in a depth range to 11 km, below which it increases with depth, in the hydrostatic pore pressure regime. The increase in $1/c_2$ with depth is ascribed to the effect of temperature. This is confirmed in Figure 16, which shows a plot of $1/c_2$ ($= D_c^{eff}/D_a$) against temperature for the data shown in Figure 15. Figure 16 also confirms that $1/c_2$ at temperatures above 300°C is more sensitively affected in the suprahydrostatic pore pressure regime than in the hydrostatic pore pressure regime. This fact indicates that the effect of water is more enhanced at temperatures higher than 300°C. Whether or not K and m depend on temperature (or the corresponding crustal depth) above 300°C is beyond the scope of the present paper, and will be left for a future study.

6. Conclusions

[40] The earthquake rupture process at shallow crustal depths is not a simple one of frictional slip failure on a precut weak fault, but a more complex process including the fracture of initially intact rock on an inhomogeneous fault. The constitutive law for earthquake ruptures must therefore be formulated as a unifying law that governs not only frictional slip failure at precut interface (or frictional contact) areas on faults but also shear fracture of intact rock at local strong areas on the faults. This leads to the conclusion that the governing law should be formulated as a slip-dependent constitutive law. In the framework of slip-dependent constitutive formulation, we have investigated by taking a numerical approach, how dimensionless constitutive law parameters S, A, and B at strong areas called "asperities" on faults are affected by the seismogenic, crustal conditions of the effective normal stress, pore pressure and temperature, and thereby estimated how these parameters vary with depth, using experimental data [*Kato et al.*, 2003a] obtained at crustal conditions simulated in the laboratory. It has been found that S gradually decreases with crustal depth and that it is greater in the suprahydrostatic pore pressure regime than in the hydrostatic pore pressure regime, due to an increase in the effective normal stress with depth. It has also been found that A decreases with depth, while B slightly increases with depth, in both the hydrostatic and suprahydrostatic pore pressure regimes. The changes in A and B with depth are ascribed to an increase in the effective normal stress with depth, and these changes in A and B with depth in the hydrostatic pore pressure regime clearly differ from those in the suprahydrostatic pore pressure regime. Though D_a and D_c^{eff} are scale-dependent, the ratio D_c^{eff}/D_a is neither scale-dependent nor dependent on ambient conditions such as the effective normal stress, pore pressure, and temperature, and it does not vary with depth and has a universal, constant value of roughly 5, in a depth range to roughly 10 km (brittle regime). At greater depths, D_c^{eff}/D_a increases with depth due to the effect of temperature on D_c^{eff}, and its increase is greater in the suprahydrostatic pore pressure regime than in the hydrostatic pore pressure regime. Reflecting these changes in S, A, and B with depth, the constitutive behavior including the slip-weakening phase distinctively varies with depth, and this behavior in the suprahydrostatic pore pressure regime clearly differs from that in the hydrostatic pore pressure regime. These results are suited for implementation in a numerical code, and they will be easily assimilated into numerical models of earthquake ruptures for realistic computer simulation.

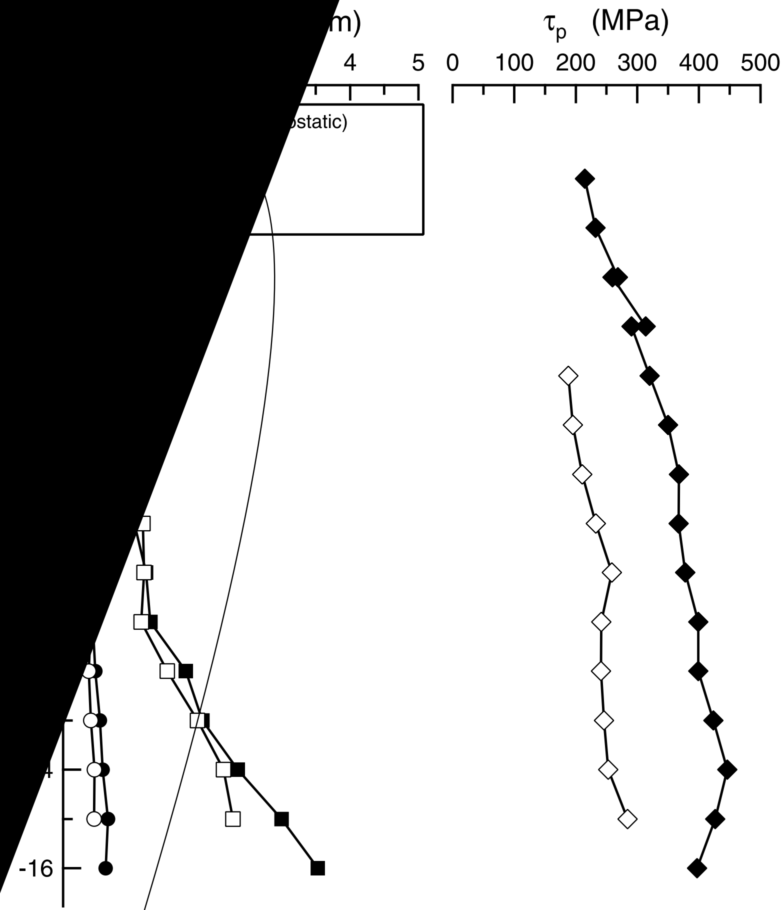

m)
4
5
ostatic)
-16
τ_p (MPa)
0
100
200
300
400
500

[41] **Acknowledgments.** The original manuscript was completed while the senior author was a visiting scholar of the Kavli Institute for Theoretical Physics, University of California at Santa Barbara, to participate in the program entitled ‘‘From the Atomic to the Tectonic: Friction, Fracture and Earthquake Physics’’ organized by James Dieterich, Michael Falk, and Mark Robbins, to whom the senior author is grateful for their invitation. This research was supported in part by the National Science Foundation under grant PHY99-07949. KITP preprint NSF-KITP-05-113. We are grateful to Jeffrey McGuire (Associate Editor) and two reviewers for their helpful comments, which greatly contributed to improving the original manuscript. We are also grateful to Mary Rose Reade for her help in enhancing the readability of the paper.

References

Aki, K. (1979), Characterization of barriers on an earthquake fault, *J. Geophys. Res.*, *84*, 6140–6148.

Aki, K. (1984), Asperities, barriers, characteristic earthquakes and strong motion prediction, *J. Geophys. Res.*, *89*, 5867–5872.

Aviles, C. A., C. H. Scholz, and J. Boatwright (1987), Fractal analysis applied to characteristic segments of the San Andreas fault, *J. Geophys. Res.*, *92*, 331–344.

Beroza, G. C., and T. Mikumo (1996), Short slip duration in dynamic rupture in the presence of heterogeneous fault properties, *J. Geophys. Res.*, *101*, 22,449–22,460.

Blanpied, M. L., D. A. Lockner, and J. D. Byerlee (1991), Fault stability inferred from granite sliding experiments at hydrothermal conditions, *Geophys. Res. Lett.*, *18*, 609–612.

Blanpied, M. L., D. A. Lockner, and J. D. Byerlee (1995), Frictional slip of granite at hydrothermal conditions, *J. Geophys. Res.*, *100*, 13,045–13,064.

Bouchon, M. (1997), The state of stress on some faults of the San Andreas system as inferred from near-field strong motion data, *J. Geophys. Res.*, *102*, 11,731–11,744.

Bouchon, M., H. Sekiguchi, K. Irikura, and T. Iwata (1998), Some characteristics of the stress field of the 1995 Hyogo-ken Nanbu (Kobe) earthquake, *J. Geophys. Res.*, *103*, 24,271–24,282.

Byerlee, J. D. (1967), Theory of friction based on brittle fracture, *J. Appl. Phys.*, *38*, 2928–2934.

Dieterich, J. H. (1978), Preseismic fault slip and earthquake prediction, *J. Geophys. Res.*, *83*, 3940–3948.

Dieterich, J. H. (1979), Modeling of rock friction: 1. Experimental results and constitutive equations, *J. Geophys. Res.*, *84*, 2161–2168.

Dieterich, J. H. (1981), Constitutive properties of faults with simulated gouge, in *Mechanical Behavior of Crystal Rocks*, *Geophys. Monogr. Ser.*, vol. 24, edited by N. L. Cater et al., pp. 103–120, AGU, Washington, D. C.

Dieterich, J. H. (1986), A model for the nucleation of earthquake slip, in *Earthquake Source Mechanics*, *Geophys. Monogr. Ser.*, vol. 37, edited by S. Das, J. Boatwright, and C. H. Scholz, pp. 37–47, AGU, Washington, D. C.

Ellsworth, W. L., and G. C. Beroza (1995), Seismic evidence for an earthquake nucleation phase, *Science*, *268*, 851–855.

Ida, Y. (1972), Cohesive force across the tip of a longitudinal-shear crack and Griffith's specific surface energy, *J. Geophys. Res.*, *77*, 3796–3805.

Ida, Y. (1973), The maximum acceleration of seismic ground motion, *Bull. Seismol. Soc. Am.*, *63*, 959–968.

Ide, S., and M. Takeo (1997), Determination of constitutive relations of fault slip based on seismic wave analysis, *J. Geophys. Res.*, *102*, 27,379–27,391.

Kanamori, H., and G. S. Stewart (1978), Seismological aspects of the Guatemala earthquake of February 4, 1976, *J. Geophys. Res.*, *83*, 3427–3434.

Kato, A., and M. Ohnaka (2000), Effect of water on stability or instability of the shear fracture process of rock (in Japanese), *J. Geography*, *109*, 554–563.

Kato, A., M. Ohnaka, and H. Mochizuki (2003a), Constitutive properties for the shear failure of intact granite in seismogenic environments, *J. Geophys. Res.*, *108*(B1), 2060, doi:10.1029/2001JB000791.

Kato, A., M. Ohnaka, S. Yoshida, and H. Mochizuki (2003b), Effect of strain rate on constitutive properties for the shear failure of intact granite in seismogenic environments, *Geophys. Res. Lett.*, *30*(21), 2108, doi:10.1029/2003GL018372.

Kato, A., S. Yoshida, M. Ohnaka, and H. Mochizuki (2004), The dependence of constitutive properties on temperature and effective normal stress in seismogenic environments, *Pure Appl. Geophys.*, *161*, 1895–1913.

Lay, T., H. Kanamori, and L. Ruff (1982), The asperity model and the nature of large subduction zone earthquakes, *Earthquake Predict. Res.*, *1*, 3–71.

Matsu'ura, M., H. Kataoka, and B. Shibazaki (1992), Slip-dependent friction law and nucleation processes in earthquake rupture, *Tectonophysics*, *211*, 135–148.

Mikumo, T., K. B. Olsen, E. Fukuyama, and Y. Yagi (2003), Stress-breakdown time and slip-weakening distance inferred from slip-velocity functions on earthquake faults, *Bull. Seismol. Soc. Am.*, *93*, 264–282.

Odedra, A. (1998), Laboratory studies on shear fracture of granite under simulated crustal conditions, Ph.D. thesis, 269 pp., Univ. College London, London.

Odedra, A., M. Ohnaka, H. Mochizuki, and P. Sammonds (2001), Temperature and pore pressure effects on the strength of granite in the brittle-plastic transition regime, *Geophys. Res. Lett.*, *28*, 3011–3014.

Ohnaka, M. (1996), Nonuniformity of the constitutive law parameters for shear rupture and quasistatic nucleation to dynamic rupture: A physical model of earthquake generation processes, *Proc. Natl. Acad. Sci. U.S.A.*, *93*, 3795–3802.

Ohnaka, M. (2000), A physical scaling relation between the size of an earthquake and its nucleation zone size, *Pure Appl. Geophys.*, *157*, 2259–2282.

Ohnaka, M. (2003), A constitutive scaling law and a unified comprehension for frictional slip failure, shear fracture of intact rock, and earthquake rupture, *J. Geophys. Res.*, *108*(B2), 2080, doi:10.1029/2000JB000123.

Ohnaka, M. (2004), Earthquake cycles and physical modeling of the process leading up to a large earthquake, *Earth Planets Space*, *56*, 773–793.

Ohnaka, M. (2006), Reply to ‘‘Comment on ‘Earthquake cycles and physical modeling of the process leading up to a large earthquake,’’’ *Earth Planets Space*, *58*, 1529–1531.

Ohnaka, M., and L. Shen (1999), Scaling of the shear rupture process from nucleation to dynamic propagation: Implications of geometric irregularity of the rupturing surfaces, *J. Geophys. Res.*, *104*, 817–844.

Ohnaka, M., and T. Yamashita (1989), A cohesive zone model for dynamic shear faulting based on experimentally inferred constitutive relation and strong motion source parameters, *J. Geophys. Res.*, *94*, 4089–4104.

Ohnaka, M., Y. Kuwahara, and K. Yamamoto (1987), Constitutive relations between dynamic physical parameters near a tip of the propagating slip zone during stick-slip shear failure, *Tectonophysics*, *144*, 109–125.

Ohnaka, M., M. Akatsu, H. Mochizuki, A. Odedra, F. Tagashira, and Y. Yamamoto (1997), A constitutive law for the shear failure of rock under lithospheric conditions, *Tectonophysics*, *277*, 1–27.

Okubo, P. G., and K. Aki (1987), Fractal geometry in the San Andreas fault system, *J. Geophys. Res.*, *92*, 345–355.

Palmer, A. C., and J. R. Rice (1973), The growth of slip surfaces in the progressive failure of over-consolidated clay, *Proc. R. Soc. London, Ser. A*, *332*, 527–548.

Papageorgiou, A. S., and K. Aki (1983), A specific barrier model for the quantitative description of inhomogeneous faulting and the prediction of strong ground motion. part II. Applications of the model, *Bull. Seismol. Soc. Am.*, *73*, 953–978.

Ruina, A. (1983), Slip instability and state variable friction laws, *J. Geophys. Res.*, *88*, 10,359–10,370.

Segall, P., and D. D. Pollard (1980), Mechanics of discontinuous faults, *J. Geophys. Res.*, *85*, 4337–4350.

Sibson, R. H. (1977), Fault rocks and fault mechanisms, *J. Geol. Soc. London*, *133*, 191–213.

Sibson, R. H. (1986), Rupture interaction with fault jogs, *Earthquake Source Dynamics*, *Geophys. Monogr. Ser.*, vol. 37, edited by S. Das, J. Boatwright, and C. H. Scholz, pp. 157–167, AGU, Washington, D. C.

Tse, S. T., and J. R. Rice (1986), Crustal earthquake instability in relation to the depth variation of frictional slip properties, *J. Geophys. Res.*, *91*, 9452–9472.

Wesnousky, S. G. (1988), Seismological and structural evolution strike-slip faults, *Nature*, *335*, 340–343.

Yamanaka, Y., and M. Kikuchi (2004), Asperity map along the subduction zone in northeastern Japan inferred from regional seismic data, *J. Geophys. Res.*, *109*, B07307, doi:10.1029/2003JB002683.

Zhang, W., T. Iwata, and K. Irikura (2003), Heterogeneous distribution of the dynamic source parameters of the 1999 Chi-Chi, Taiwan, earthquake, *J. Geophys. Res.*, *108*(B5), 2232, doi:10.1029/2002JB001889.

A. Kato, Earthquake Research Institute, University of Tokyo, Bunkyo-ku, Tokyo 113-0032, Japan.

M. Ohnaka, Utsukushigaoka-nishi 3-40-19, Aoba-ku, Yokohama 225-0001, Japan. (ohnaka@g05.itscom.net)